

Triazolyl-Functionalized *N*-Heterocyclic Carbene Half-Sandwich Compounds: Coordination Mode, Reactivity and *in vitro* Anticancer Activity

Kelvin K. H. Tong,^[a, b] Muhammad Hanif,^[a, b] Sanam Movassaghi,^[a] Matthew P. Sullivan,^[a, b, c] James H. Lovett,^[d] Katja Hummitzsch,^[e] Tilo Söhnel,^[a] Stephen M. F. Jamieson,^[b, f] Suresh K. Bhargava,^[g] Hugh H. Harris,^[d] and Christian G. Hartinger*^[a, b]

We report investigations on the anticancer activity of organometallic $[M^{II/III}(\eta^6\text{-}p\text{-cymene}/\eta^5\text{-pentamethylcyclopentadienyl})]$ ($M = \text{Ru, Os, Rh, and Ir}$) complexes of *N*-heterocyclic carbenes (NHCs) substituted with a triazolyl moiety. Depending on the precursors, the NHC ligands displayed either mono- or bidentate coordination *via* the NHC carbon atom or as *N,C*-donors. The metal complexes were investigated for their stability in aqueous solution, with the interpretation supported by density functional theory calculations, and reactivity to

biomolecules. *In vitro* cytotoxicity studies suggested that the nature of both the metal center and the lipophilicity of the ligand determine the biological properties of this class of compounds. The Ir^{III} complex **5d** bearing a benzimidazole-derived ligand was the most cytotoxic with an IC₅₀ value of 10 μM against NCI-H460 non-small cell lung carcinoma cells. Cell uptake and distribution studies using X-ray fluorescence microscopy revealed localization of **5d** in the cytoplasm of cancer cells.

Introduction

Upon coordination to transition metals *N*-heterocyclic carbene (NHC) ligands offer σ -donating as well as π -accepting properties to form strong M–L bonds.^[1] The inferred stability of M–NHC complexes is advantageous for a variety of applications, including in homogeneous catalysis.^[2]

More recently, metal–NHC complexes have been investigated as potential drug candidates, including as anticancer and antibacterial agents.^[3] The NHC scaffold derived from azolium pro-carbenes, most commonly imidazolium derivatives, offers facile routes for modification, allowing the fine-tuning of the physicochemical properties and biological activity of metal–NHC complexes.^[3c,d] Ag(NHC) compounds were among the first metal–NHC complexes found to exhibit biological activity.^[4] In addition to their antimicrobial activity, some examples showed promising anticancer properties comparable to that of cisplatin.^[4b,5] Au(NHC) complexes induced Ca²⁺-sensitive mitochondrial swelling, and the onset of mitochondrial swelling was dependent on the lipophilicity of the compound, which was influenced by the *N*-substituents of the NHC moiety.^[6] Ru^{II}(arene) complexes and their isostructural Os^{II}(arene), Ir^{III}(Cp*), and Rh^{III}(Cp*) (Cp* = η^5 -pentamethylcyclopentadienyl) analogs showed anticancer activity in some cases, seemingly dependent on the lipophilicity of the complexes as evoked by the substitution pattern of the NHC moiety.^[3b,d,7] Furthermore, surprising reactivity was observed, particularly in the presence of proteins.^[8] Some examples exhibited antiproliferative effects and inhibited thioredoxin reductase,^[3d,7b,9] similar to Au^I(NHC) complexes.^[10]

By incorporating a chelating NHC ligand, additional functionality can be introduced into metal–NHC complexes, as well as enhancing their stability. Several Ir^{III}(Cp*) complexes with C,C-, C,N-, and C,O-coordinating NHC ligands exhibited moderate to high antitumor activity against cancer cells.^[11] The cytotoxic activity of the C,N-coordinated complexes was further improved by altering the substituents of the Cp* and chelating NHC ligands, to become 3-times more potent than cisplatin. Furthermore, a Ru^{II}(cym) complex featuring a chelating pyrazole-NHC ligand was a highly efficient catalyst for alcohol

[a] K. K. H. Tong, Dr. M. Hanif, Dr. S. Movassaghi, Dr. M. P. Sullivan, Prof. T. Söhnel, Prof. C. G. Hartinger
School of Chemical Sciences, University of Auckland
Private Bag 92019, Auckland 1142 (New Zealand)
E-mail: c.hartinger@auckland.ac.nz

[b] K. K. H. Tong, Dr. M. Hanif, Dr. M. P. Sullivan, Dr. S. M. F. Jamieson, Prof. C. G. Hartinger
Maurice Wilkins Centre, University of Auckland
Private Bag 92019, Auckland 1142 (New Zealand)

[c] Dr. M. P. Sullivan
School of Biological Sciences, University of Auckland
Private Bag 92019, Auckland 1142 (New Zealand)

[d] J. H. Lovett, Prof. H. H. Harris
Department of Chemistry, The University of Adelaide
Adelaide, SA 5005 (Australia)

[e] Dr. K. Hummitzsch
Discipline of Obstetrics and Gynecology
The University of Adelaide
Robinson Research Institute, Adelaide, SA 5005 (Australia)

[f] Dr. S. M. F. Jamieson
Auckland Cancer Society Research Centre
University of Auckland
Private Bag 92019, Auckland 1142 (New Zealand)

[g] Prof. S. K. Bhargava
Centre for Advanced Materials and Industrial Chemistry
School of Science, RMIT University, Melbourne (Australia)

 Supporting information for this article is available on the WWW under <https://doi.org/10.1002/cmdc.202100311>

 This article belongs to the joint Special Collection with the European Journal of Inorganic Chemistry, "Metals in Medicine".

oxidation as well as displaying significant cytotoxicity against cisplatin-resistant gastric cancer cells.^[12]

One method to introduce new functionality into imidazolium-derived NHC complexes is to alkylate an endocyclic nitrogen atom of the imidazole precursor with an alkyne followed by click chemistry using the copper(I)-catalyzed azide-alkyne cycloaddition (CuAAC). The resultant triazolyl moiety converts the pro-carbene into a chelating ligand, which coordinates to metal centers in *C,C*- or *C,N*-bidentate fashion.^[13] While the catalytic properties of a diversity of complexes with such ligands were studied for different catalytic applications,^[13a,c] the bioactivity was rarely investigated. We have previously reported a series of cationic Ru^{II}(cym) complexes (cym = 1⁶-*p*-cymene) featuring *C,N*-coordinating NHC-pyridyl ligands that formed 5- and 6-membered metallacycles upon coordination to the Ru^{II} center.^[14] Some of these complexes showed potent antiproliferative activity with IC₅₀ values in the low μM range. Herein, we expand on the compound type and explore the impact of the metal center and denticity of the ligand on the antiproliferative activity. These investigations are complemented by studies on the aqueous stability and reactivity toward biomolecules as well as their intracellular distribution.

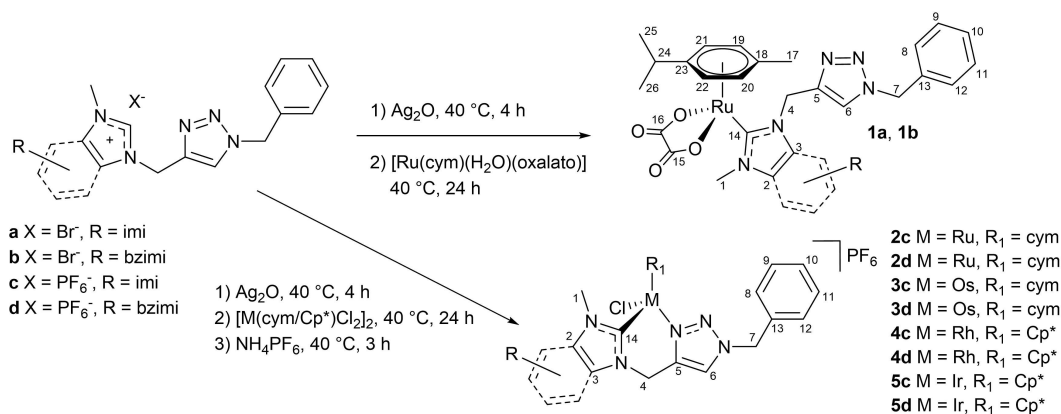
Results and Discussion

CuAAC was utilized to prepare the 1,2,3-triazolyl-NHC precursors **a** and **b** from 1-methyl-3-propargylimidazolium bromide and 1-methyl-3-propargylbenzimidazolium bromide.^[15] Successful conversion was confirmed by ¹H and ¹³C{¹H} NMR spectroscopy, electrospray ionization mass spectrometry (ESI-MS), and elemental analysis. The carbenic carbon and the triazolyl nitrogen atoms enable **a** and **b** to act either as mono- or bidentate ligands to metal centers. [Ru^{II}(cym)(H₂O)(oxalato)] was used as a metal precursor to synthesize complexes with the NHC ligand acting as a monodentate ligand and the remaining coordination sites of the Ru^{II} center occupied by the bidentate oxalato group. Formation of the carbene by addition of Ag₂O directs the coordination of **a** or **b** to the metal center *via* the

carbenic carbon of the imidazole moiety (Scheme 1), yielding **1a** and **1b** in low yields (28 and 30%, respectively).

Messerle and co-workers^[13a,c] reported *C,N*-coordinated NHC-triazolyl half-sandwich complexes including the Rh- and Ir(Cp* compounds **4c** and **5c** (Scheme 1). Using the same ligand type, we expanded on the series and prepared ligands from the corresponding [M^{III}(cym/Cp*)Cl₂]₂ dimers (M = Ru, Os, Rh, Ir) and the respective pro-carbenes (Scheme 1). NH₄PF₆ was added to facilitate counterion metathesis of Cl⁻ with PF₆⁻. In initial attempts, nearly stoichiometric amounts of Ag₂O, pro-carbene, and [Ru^{II}(cym)Cl₂]₂ were used for the preparation of **1a** and **1b**. However, analysis of the products by ¹H NMR spectroscopy revealed the formation of only small amounts of the desired product and traces of unreacted Ag^I(NHC) intermediate and dimeric metal precursors. The stoichiometry of the reaction mixture was optimized and identified as 2.25:1.375:1.0 (pro-carbene:Ag₂O:[M^{III}(cym/Cp*)Cl₂]₂) for preparation of the desired Ru^{II}- and Os^{II}(NHC) complexes **2c** and **3c**, respectively, at high purity although low to moderate yields. The same synthetic approach was unsuccessful in the preparation of the Rh- and Ir^{III}(Cp*) derivatives **4c** and **5c**. The ESI-mass spectra indicated the presence of the bromido complex (Supporting Information) as both pro-carbenes **a** and **b** were prepared as the bromide salts. To eliminate the bromide ions in subsequent syntheses, **a** and **b** were converted into the hexafluorophosphate salts **c** and **d**, respectively. The counterion metathesis of bromide to PF₆⁻ was confirmed by ³¹P NMR spectroscopy (data not shown). This process allowed the subsequent reaction steps to proceed successfully to yield complexes **2c–5d** (17–66%) in high purity.

The synthesized metal complexes were characterized by NMR spectroscopy, ESI-MS, and elemental analysis. In the ¹H NMR spectra of **1a** and **1b**, the absence of the pro-carbene proton signal and the slight upfield shift of the triazolyl proton signal from 8.45 to 8.40 ppm and 8.60 to 8.40 ppm, respectively, was considered indicative of NHC complex formation. In the case of **2c–5d**, the triazolyl proton signals experienced significant upfield shifts and were detected in the range of 7.68–8.07 ppm. Furthermore, the absence of the pro-carbene proton signal of the imidazolium and benzimidazolium precursors



Scheme 1. Preparation of the [Ru^{II}(cym)(NHC)(oxalato)] complexes **1a** and **1b**, and of the [M(cym/Cp*)(triazolyl-NHC)Cl]PF₆ complexes **2c–5d**.

sors suggested that both **c** and **d** coordinated to the metal centers through the carbenic carbon and the triazolyl nitrogen atoms to establish a six-membered metallaring. Upon metal coordination, the signals of the two sets of bridging methylene protons in the range of 4.83–5.75 ppm became diastereotopic and showed geminal coupling. Furthermore, the differences in the chemical shifts of the diastereotopic methylene proton signals were higher for those being part of the metallaring, with $^2J_{\text{H-H}}$ values ranging from 14 to 17 Hz. The latter were difficult to assign due to overlapping of these signals with the cym resonances. In the $^{13}\text{C}\{^1\text{H}\}$ NMR spectra, the carbenic carbon atom resonated in complexes at significantly lower field (153–188 ppm) compared to the pro-carbenes (138–142 ppm). In both **4c** and **4d**, the signals corresponding to the carbon atoms bonded to the Rh center were detected as doublets (Rh–C_{NHC}, $^1J = 50$ Hz; Rh–C_{Cp*}, $^1J = 7$ Hz). ESI-MS studies further confirmed the identity of the NHC complexes. The Ru^{II}(oxalato) complexes **1a** and **1b** were detected as $[\text{M} + \text{Na}]^+$ and **2c–5d** as $[\text{M} - \text{PF}_6]^-$ pseudomolecular ions (Table S1). The elemental analysis results indicated the presence of small amounts of solvent for some complexes, and these solvents were evident in the ^1H NMR spectra.

Single crystals suitable for X-ray diffraction analysis of **1b**, **2c**^{Cl}, and **2d**^{Cl} were grown *via* slow diffusion of toluene into saturated solutions in acetonitrile. In contrast, crystals of **5c** were obtained from a reaction mixture containing L-histidine, water, methanol, and **5d** in chloroform *via* slow evaporation. Note that the single crystals of **2c**^{Cl} and **2d**^{Cl} were obtained from reactions between $[\text{Ru}(\text{cym})\text{Cl}_2]_2$ and **c** and **d**. Complexes **1b** and **5c** crystallized in the triclinic space group *P*-1, while **2c**^{Cl}, **2d**^{Cl}, and **5d** were detected in the monoclinic space groups *P*2₁/*c*, *C*2/*c*, and *P*2₁, respectively (Table S2). Complexes **2c**^{Cl}, **2d**^{Cl}, and **5c** featuring non-symmetric bidentate ligands crystallized as enantiomeric mixtures with a prochiral metal center.

The complexes adopted a pseudo-octahedral configuration, where both the cym (**1b**, **2c**^{Cl}, **2d**^{Cl}) and Cp* ligands (**5c**, **5d**) occupied three coordination sites (Figures 1, S1 and S2). In the case of **1b**, the coordination sphere about the Ru center was filled with an oxalato and the NHC ligand, and for the latter π -stacking interactions were observed between two independent molecules of **1b** (3.375 Å). The molecular structures of **2c**^{Cl}, **2d**^{Cl}, **5c**, and **5d** demonstrated the expected bidentate coordination of the triazole-functionalized NHC ligand to the metal center *via* the M–C_{NHC} and M–N3 bonds. This resulted in the formation of 6-membered metallacycles with distorted boat conformation. Complexes **2c**^{Cl}, **2d**^{Cl}, **5c**, and **5d** showed shorter M–C_{NHC} bonds compared to **1b** (Table 1). In isostructural **2c**^{Cl}, **2d**^{Cl}, **5c**, and **5d**, the M–Cl bond length in **2d**^{Cl} was significantly longer than for the other compounds, while the M–C_{NHC} and M–N3 were the shortest of the series and similar to related metal-NHC complexes.^[14]

The Ru–N3 bond length of **2c**^{Cl} and **2d**^{Cl} was compared to a series of Ru^{II}(η^6 -benzene) complexes featuring a similar bidentate ligand with a triazolyl moiety coordinating to the Ru center through the N3 atom.^[16] The distance of Ru–N3 of these complexes is on average 2.09 Å, which is longer than that of **2c**^{Cl} and **2d**^{Cl}. The bond length differences may be attributed to

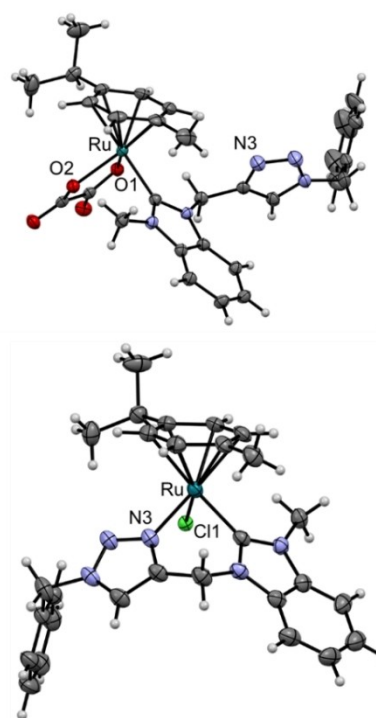


Figure 1. ORTEP representations of the molecular structures of **1b** and one of the enantiomers of **2d**^{Cl} (bottom), drawn at 50% ellipsoid levels. Any counterions and solvent molecules were omitted for clarity.

Table 1. Key bond lengths for **1b**, **2c**^{Cl}, **2d**^{Cl}, **5c**, and **5d**.

Complex	1b	2c ^{Cl}	2d ^{Cl}	5c	5d
			Bond length [Å]		
M–Cl	–	2.4287(7)	2.4435(9)	2.409(2)	2.412(1)
M–C _{NHC}	2.072(3)	2.062(3)	2.035(3)	2.026(9)	2.035(8)
M–N3	–	2.084(2)	2.068(3)	2.087(7)	2.077(5)
M–R _{1,centroid}	1.690	1.706	1.698	1.825	1.814

the 5-membered metallacycle as well as involving S or Se as the other donor atom of the bidentate ligand.^[16]

In **5c**, protons of the imidazole moiety, methylene linker, and triazole moiety showed interactions with a PF₆[–] counterion. Interactions with PF₆[–] ions were also observed for **5d** but involving triazole, methylene, and benzyl protons. The distances of the observed C–H...F interactions ranged from 2.3 to 2.8 Å, which is in accordance with values reported for a series of imidazole-thione complexes (Supporting Information, Figure S2).^[17]

Organometallics with metal-halido bonds may undergo ligand exchange reactions in biologically relevant environments, such as in water or DMSO, the latter commonly used to prepare stock solutions for compounds with low aqueous solubility. Therefore, it is essential to investigate the stability of the metal complexes in various solvents. ^1H NMR spectroscopic studies were conducted for **2c–5c** in 15% DMSO-*d*₆/D₂O for 120 h (Figures S3–S6, Table S3). The formation of aqua species was confirmed experimentally by adding 1.5 molar equivalents of AgNO₃ to the reaction mixtures and comparing the

respective ^1H NMR spectra. Compounds **2c** and **3c** underwent immediate $\text{Cl}^-/\text{H}_2\text{O}$ ligand exchange to form the respective aqua complexes (Figures S3 and S4). Dissolution of **4c** in 15% $\text{DMSO-}d_6/\text{D}_2\text{O}$ results in the formation of several sets of signals, presumably a mixture of the chlorido **4c**, aqua $4c^{\text{H}_2\text{O}}$, and $\text{DMSO } 4c^{\text{DMSO}}$ complexes, which form an equilibrium rapidly after dissolution (Figure S5). The addition of AgNO_3 changed the distribution of the signal sets by converting the chlorido into an aqua complex. In contrast to the other imidazole-based complexes, gradual $\text{Cl}^-/\text{H}_2\text{O}$ ligand exchange was observed for the Ir derivative **5c**, where about 18% of $5c^{\text{H}_2\text{O}}$ was formed upon dissolution and went to completion within 3 h (Figure S6), as confirmed by the addition of AgNO_3 (Figure 2). Furthermore, an aged solution of **5c** in $\text{DMSO-}d_6$ was diluted with D_2O and analyzed which also demonstrated that aqua species are formed rather than the DMSO complex (Figure S7). This was supported by a ^1H NMR spectroscopic study in CDCl_3 to which several equivalents of DMSO were added and no DMSO complexes were detectable after 4 h (Figure S8).

The $\text{Cl}^-/\text{H}_2\text{O}$ ligand exchange of **2c–5c** was investigated with density functional theory (DFT) calculations using GAUSSIAN 09 W.^[18] For all cases, the calculated energy difference was slightly positive for $\text{Cl}^-/\text{H}_2\text{O}$ ligand exchange (ΔE range = 2.5–4.6 kcal/mol) and negative for Cl^-/OH^- ligand exchange (ΔE ranging from –55.0 to –60.3 kcal/mol). This result suggested that the formation of the hydroxido complexes is more energetically favorable, which would give a singly charged rather than a doubly charged complex cation. Similar calculated energy differences were observed in a series of structurally related $\text{Ru}(\text{NHC})$ complexes.^[14] The frontier molecular orbitals of **2c–5c** and their respective aqua and hydroxido analogs were analyzed (Figures S9–12). While in the respective chlorido and aqua species the HOMOs and LUMOs are located mainly on the metal and its π -bound ligands, the LUMO in **3c** is distributed over the metal center and the triazole moiety. In general, the π orbitals of the triazolyl group contributed more extensively to the LUMOs of the compounds than to the HOMOs, independent of the nature of the monodentate ligand.

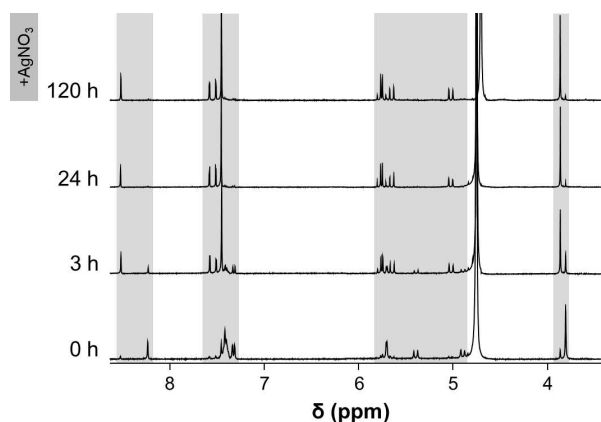


Figure 2. Time-dependent ^1H NMR spectroscopic stability study for **5c** in 15% $\text{DMSO-}d_6/\text{D}_2\text{O}$ over 120 h.

Metal complexes are prone to form dative covalent bonds to donor atoms of biomolecules. Investigating the interactions between metallodrugs and biomolecules can provide valuable data to help determine possible modes of action responsible for any antiproliferative effects. To study the interactions with biomolecules, **2c–5c** were dissolved in 20% $\text{MeOD}_4/\text{D}_2\text{O}$ and one equivalent of L-cysteine (Cys), L-methionine (Met), L-histidine (His), or 9-ethylguanine (EtG) was added. The reaction mixtures were analyzed by ^1H NMR spectroscopy over a period of 48 h. Complex **2c** showed only minor reactions with the amino acids and EtG (Figures S13–16), while the Os analog **3c** did not form adducts with any of the nucleophiles (Figures S17–20). In contrast, the Cp^* derivatives **4c** and **5c** reacted with all the biomolecules (Figures S21–28), the latter however at a slower rate. In particular with His, several sets of signals formed, possibly due to different coordination modes (Figures S23 and S27). Notably, addition of another equivalent of His resulted in significant upfield shifts of the peaks assigned to unreacted His due to pH changes in the sample. Analysis of an incubation mixture of **5c** with Cys by ESI-MS supported the formation of a **5c–Cys** adduct, which was detected as the $[\text{5c–Cl–H+Cys}]^+$ ion at m/z 702.2324 (m/z_{theory} 702.2322), while the formation of a **5c–EtG** adduct was indicated by a signal emerging at around 8.0 ppm in the ^1H NMR spectrum, which can be assigned to H8 of EtG coordinated to the Ir center (Figure 3). The EtG adduct formation was confirmed by ESI-MS and the pseudomolecular ion $[\text{5c–Cl–H+EtG}]^+$ with m/z 759.2781 (m/z_{theory} 759.2859) was detected.

The *in vitro* anticancer activity of the complexes and pro-NHCs was studied against human cervical carcinoma (SiHa), colon adenocarcinoma (SW480), colorectal (HCT116), and non-small-cell lung (NCI-H460) cancer cells (Table 2). The compounds demonstrated variable cytotoxic activity with IC_{50} values as low as 10 μM for some derivatives, while others were non-cytotoxic at the concentrations investigated. The pro-NHC **c** was inactive and **d** only showed minor activity in NCI-H460 and SiHa cells. The Ir^{III} compounds **5c** and **5d** demonstrated significantly

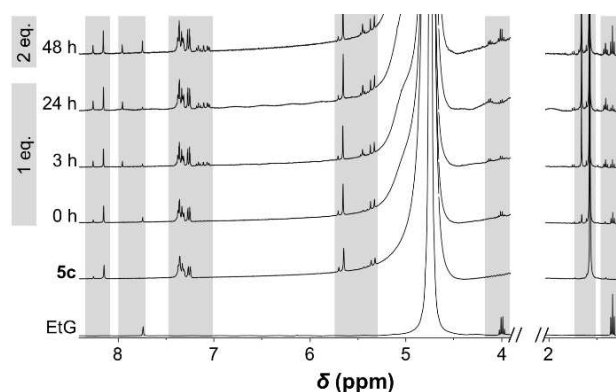


Figure 3. Time-dependent ^1H NMR spectroscopic stability study of the reaction between equimolar amounts of **5c** and EtG in 20% $\text{MeOD}/\text{D}_2\text{O}$ solution over 48 h. An additional molar equivalent of EtG was added after 48 h to indicate unreacted EtG in solution. Grey boxes denote the change in the chemical shifts of the proton signals of **5c** as the result of reacting with EtG in solution.

Table 2. Antiproliferative activity (SRB assay, 72 h treatment) expressed as the IC_{50} values (μM) for pro-carbenes **c** and **d**, and complexes **1a–5d** against HCT116 (human colorectal carcinoma), NCI-H460 (human non-small cell lung carcinoma), SiHa (human cervical carcinoma), and SW480 (human colon adenocarcinoma) cancer cells expressed as mean \pm standard error ($n=3$).

Compound	IC_{50} values [μM]			
	HCT116	NCI-H460	SiHa	SW480
c	> 100	> 100	> 100	> 100
1a	> 100	> 100	> 100	> 100
2c	> 100	> 100	80 ± 48	> 100
3c	> 100	> 100	81 ± 5	> 100
4c	> 100	> 100	> 100	> 100
5c	36 ± 1	21 ± 6	12 ± 2	70 ± 19
d	> 100	78 ± 6	78 ± 15	> 100
1b	> 100	> 100	> 100	> 100
2d	> 100	> 100	> 100	> 100
3d	> 100	> 100	> 100	> 100
4d	91 ± 8	66 ± 18	64 ± 1	95 ± 6
5d	17 ± 2	10 ± 1	13 ± 1	26 ± 4

higher cytotoxicity in all cell lines than the compounds with the other metal centers, with benzimidazole-derived **5d** being the most toxic compound against all cell lines (Figure S29). This may be due to the relatively slower $\text{Cl}^-/\text{H}_2\text{O}$ ligand exchange kinetics of Ir complexes, as demonstrated for **5c**.

The most cytotoxic compound **5d** was selected for further investigations on its uptake and localization in human lung cancer A549 and ovarian cancer SKOV-3 cells by X-ray fluorescence microscopy (XFM) (Figure 4). After treating the cells with **5d** ($30 \mu\text{M}$ in 1% DMSO) for 4 h, the confocal images confirmed that the cells remained intact indicating that the uptake of the metal complex occurred while the cells were alive. The high quantities of zinc in cell nuclei enable it to be easily identified in XFM studies.^[19] The Ir complexes were taken up into the cells, while control experiments showed no signal for Ir in untreated cells (data not shown). The cellular uptake of **5d** was consistently observed for both cell lines as indicated by the relatively similar Zn/Ir elemental concentration ratio. By overlaying the distribution of Zn and Ir in the cells, no co-localization was observed which suggests that **5d** is taken up into the cytoplasm of SKOV-3 and A549 cells rather than the

nuclei. Therefore, it is unlikely that nuclear DNA is the molecular target of **5d**.

Conclusion

NHC complexes have found widespread application and more recently have attracted interest in anticancer metallodrug research. We report here investigations on ligands that feature a bidentate chelation motif composed of an NHC and a triazole moiety, and their use in different synthetic strategies to prepare half-sandwich organometallic compounds with the ligands in either mono- or bidentate coordination modes. Whereas the Ru and Os complexes underwent rapid chlorido-aqua ligand exchange resulting in stable hydrolysis products, the Rh and Ir derivatives gave more complicated ^1H NMR spectra after dissolution in water/DMSO mixtures. The Ir compound converted into the aqua complex more slowly, while for the Rh derivative a mixture of adducts, most likely with water and DMSO, was observed. This pattern also translated to the biomolecule binding studies with the Ru and Os compounds undergoing only slow or no reaction with biological nucleophiles, while the Rh and Ir compounds reacted with the amino acids and EtG. The Ir derivative proceeded at a slower rate than the Rh compound, owing to the different levels of inertness. Moreover, DFT calculations suggested the formation of hydroxido complexes, which may explain both the different behavior upon dissolution in water and in terms of reactivity to biomolecules. The anticancer activity of the compounds was investigated, and the complexes in which the ligands were coordinated in a monodentate manner were inactive against human cancer cell lines. Of the complexes featuring a bidentate NHC-triazole coordination motif, the Ir(Cp^*) derivatives were the only examples that showed anticancer activity with IC_{50} values as low as $10 \mu\text{M}$ for **5d** in NCI-H460 cells. The imidazole-derived complexes were less potent than the benzimidazole analogs, suggesting that lipophilicity may impact cellular accumulation. X-ray fluorescence microscopy revealed that the most potent compound **5d** was uptaken by the cell uptake and became localized in the cytoplasm in cancer cells.

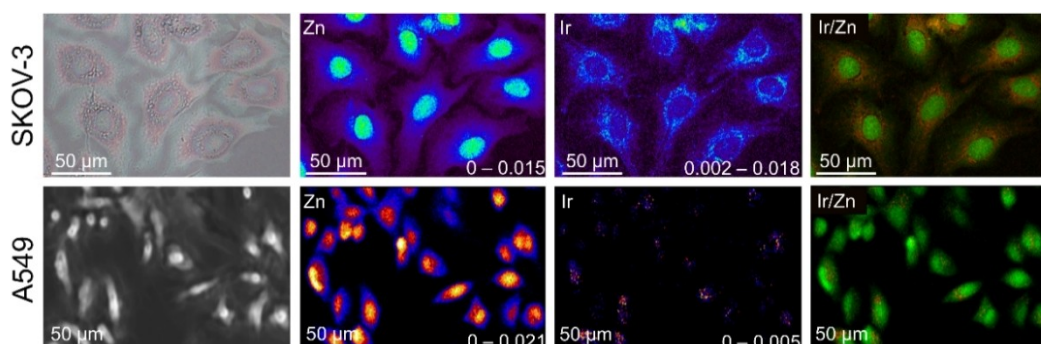


Figure 4. The distribution of Zn and Ir (heatmap color scale) in SKOV-3 and A549 cancer cells after treatment with **5d** as determined by X-ray fluorescence microscopy. The overlays of Zn and Ir distributions indicate that **5d** is accumulated in the cytoplasm instead of the cell nucleus (Zn, green; Ir, red). Elemental concentrations are given in units of $\mu\text{g cm}^{-2}$.

Experimental Section

Materials and Methods

All air-sensitive reactions were carried out under N₂ in standard Schlenk or round-bottom flasks. The complexes were prepared in darkness by covering the flask with aluminum foil to prevent photolytic degradation. Acetonitrile and dichloromethane were dried prior to use with Na₂SO₄, while all other solvents purchased from commercial suppliers were used without further purification.

1-Methylbenzimidazole (AK-Scientific, 98%), 1-methylimidazole (Acros Organic, 99%), 1,2,3,4,5-pentamethylcyclopentadiene (Merck, ≥ 88%), 9-ethylguanine (Sigma-Aldrich, 98%), ammonium hexafluorophosphate (Acros Organic, 99%), α-terpinene (Sigma-Aldrich, 89%), benzyl bromide (Merck, ≥ 98%), celite (Sigma-Aldrich), copper sulfate pentahydrate (ECP, ≥ 98.0%), L-cysteine (AK Scientific, 98%), L-histidine (AK Scientific, 98%), L-methionine (AK Scientific, 98%), iridium(III) chloride hydrate (Precious Metals Online, 99%), osmium(III) chloride hydrate (Heraeus South Africa, 55% metal content), propargyl bromide (Aldrich, 80 wt. % in toluene), rhodium(III) chloride hydrate (Precious Metals Online, 99%), ruthenium(III) chloride hydrate (Precious Metals Online, 99%), silver nitrate (Chem-supply, 99%), silver oxide (Sigma-Aldrich, 99%), sodium azide (Sigma-Aldrich, ≥ 99%), sodium L-ascorbate (Sigma-Aldrich, ≥ 98%), sodium oxalate (BDH), and sodium sulfate anhydrous (ECP, ≥ 98%) were from commercial suppliers and used as received. [Ru(cym)(H₂O)(oxalato)]^[20] and the dimeric precursors [Os(cym)Cl₂]₂,^[21] [Ru(cym)Cl₂]₂,^[22] [Ir(Cp*)Cl₂]₂,^[23] and [Rh(Cp*)Cl₂]₂^[24] were synthesized following literature procedures. Benzyl azide was prepared according to a literature procedure using ethanol:H₂O = 8:1 as the solvent mixture instead of acetone.^[25] 1-[(1-Benzyl-1,2,3-triazol-4-yl)methyl]-3-methylimidazolium bromide **a** and 1-[(1-Benzyl-1,2,3-triazol-4-yl)methyl]-3-methylbenzimidazolium bromide **b** were prepared in THF:H₂O = 1:1 as the solvent mixture instead of DMSO, as reported by others.^[13a]

Elemental analyses were conducted on a Vario EL cube (Elementar Analysensysteme GmbH, Hanau, Germany). Both 1D (¹H and ¹³C{¹H}) DEPT-Q and 2D (¹H–¹H COSY, ¹H–¹³C HSQC, and ¹H–¹³C HMBC) NMR spectra were recorded on Bruker Avance AVIII 400 MHz NMR spectrometers at 399.89 MHz (¹H) or 100.57 MHz (¹³C{¹H}) at ambient temperature in CDCl₃, DMSO-*d*₆, or D₂O. ESI-mass spectra were recorded on a Bruker micrOTOF-Q II ESI-MS in positive ion mode.

X-ray diffraction measurements of single crystals of **1 b**, **2 c**, **2 d**, **5 c**, and **5 d** were performed on a Rigaku Oxford Diffraction XtaLAB-Synergy-S single-crystal diffractometer with a PILATUS 200 K hybrid pixel array detector using Cu Kα radiation (λ = 1.54184 Å; Table S2). The data sets were processed with the SHELX2016^[26] and Olex2^[27] software packages. All non-hydrogen atoms were refined anisotropically. Hydrogen atoms were inserted at calculated positions and refined with a riding model or without restrictions. Mercury 2020.3.0 was used to visualize and generate figures of the molecular structures.^[28]

Syntheses

General procedure for the syntheses of compounds **1 a** and **1 b**

Silver(I) oxide (1.00–1.50 mol equiv.) was added to a solution of compounds **a** or **b** (1.13–1.50 mol equiv.) dissolved in dichloromethane and the mixture was stirred at 40 °C for 4 h in darkness. A solution of [Ru^{II}(oxalato)(cym)(H₂O)] (1.00–1.50 mol equiv.) dissolved in dichloromethane was added and the mixture was allowed to stir at 40 °C for 24 h in darkness. The solvents were evaporated and

dichloromethane (ca. 25 mL) was added. The resultant suspension was filtered through a celite pad (ca. 5 cm) and flushed with dichloromethane (ca. 200 mL) followed by a mixture of acetonitrile and methanol (ca. 200 mL, 8:2) as eluent which was collected containing the compound. The solvent was evaporated, the crude product was dissolved in a minimal amount of dichloromethane and the compound was precipitated by addition of *n*-hexane. The precipitate was dried *in vacuo* to obtain the pure Ru^{II}(η⁶-*p*-cymene)(oxalato) complexes.

[(Oxalato-κ²O,O')]{1-[(1-Benzyl-1,2,3-triazol-4-yl-κN)methyl]-3-methylimidazole-2-ylidene-κC}(η⁶-*p*-cymene)ruthenium(II)] **1 a**

The synthesis of **1 a** was performed according to the general procedure using **a** (115 mg, 0.34 mmol), silver(I) oxide (49 mg, 0.21 mmol), and [Ru^{II}(oxalato)(cym)(H₂O)] (104 mg, 0.30 mmol) to afford a brown powder (59 mg, 30%). Calcd. for C₂₆H₂₉N₅O₄Ru·0.2 C₆H₁₄·0.5H₂O: C, 54.19; H, 5.48; N, 11.62%. Found: C, 54.49; H, 5.16; N, 11.32%. MS (ESI⁺): *m/z* 600.1171 [M+Na]⁺ (*m*_{calc} = 600.1161). ¹H NMR (399.89 MHz, CDCl₃); δ (ppm) 8.40 (s, 1H, H-6), 7.37–7.28 (m, 5H, H-8, H-9, H-10, H-11, H-12), 7.14 (s, 1H, H-3), 6.88 (s, 1H, H-2), 5.61 (d, ²J_{H–H'} = 14 Hz, 1H, H-4a/b), 5.57 (dd, ³J = 6 Hz, ⁴J = 1.5 Hz, 1H, H-19/20), 5.55 (dd, ³J = 6 Hz, ⁴J = 1.3 Hz, 1H, H-19/20), 5.51 (d, ²J_{H–H'} = 14 Hz, 1H, H-7a/b), 5.36 (d, ²J_{H–H'} = 14 Hz, 1H, H-7a/b), 5.28 (m, 2H, H-21/22), 5.18 (d, ²J_{H–H'} = 14 Hz, 1H, H-4a/b), 3.76 (s, 1H, H-1), 2.82 (sept, ³J = 7 Hz, 1H, H-24), 2.11 (s, 3H, H-15), 1.28 (d, ³J = 6 Hz, 3H, H-25/26), 1.26 (d, ³J = 5.5 Hz, 3H, H-25/26). ¹³C {¹H} NMR (100.57 MHz, CDCl₃); δ (ppm) 174.1 (C-14), 165.8 (C-15/C-16), 165.3 (C-15/C-16), 142.8 (C-5), 134.7 (C-13), 129.1 (C-8/C-9/C-11/C-12), 128.7 (C-10), 128.5 (C-8/C-9/C-11/C-12), 125.8 (C-6), 124.2 (C-2), 122.0 (C-3), 108.7 (C-23), 97.9 (C-18), 84.7 (C21/C22), 84.1 (C21/C22), 82.1 (C19/C20), 81.6 (C19/C20), 54.5 (C-7), 45.1 (C-4), 37.6 (C-1), 31.6 (C-24), 22.9 (C25/C26), 22.5 (C25/C26), 18.8 (C-17).

[(Oxalato-κ²O,O')]{1-[(1-Benzyl-1,2,3-triazol-4-yl-κN)methyl]-3-methylbenzimidazole-2-ylidene-κC}(η⁶-*p*-cymene)ruthenium(II)] **1 b**

The synthesis of **1 b** was performed according to the general procedure using **b** (128 mg, 0.33 mmol), silver(I) oxide (47 mg, 0.20 mmol), and [Ru^{II}(oxalato)(cym)(H₂O)] (101 mg, 0.30 mmol) to afford a light brown powder (58 mg, 28%). Single crystals suitable for X-ray diffraction analysis were grown from acetonitrile/toluene. Calcd. for C₃₀H₃₁N₅O₄Ru·1.55H₂O·0.25 C₆H₁₄: C, 55.96; H, 5.61; N, 10.36%. Found: C, 56.10; H, 5.24; N, 10.00%. MS (ESI⁺): *m/z* 650.1301 [M+Na]⁺ (*m*_{calc} = 650.1317). ¹H NMR (399.89 MHz, CDCl₃); δ (ppm) 8.40 (s, 1H, H-10), 7.70 (d, ³J = 8 Hz, 1H, H-3/H-6), 7.33–7.24 (m, 7H, H-3/H-6, H-4/H-5, H-12, H-13, H-14, H-15, H-16), 7.19 (td, ³J = 8 Hz, ²J = 1.3 Hz, 1H, H-4/H-5), 5.87 (d, ²J_{H–H'} = 14 Hz, 1H, H-8a/b), 5.69–5.62 (m, 3H, H-8a/b, H-23/H-24/H-25/H-26), 5.48–5.33 (m, 4H, H-11a, H-11b, H-23/H-24/H-25/H-26), 3.97 (s, 3H, H-1), 2.86 (sept, ³J = 7 Hz, 1H, H-28), 2.11 (s, 3H, H-21), 1.28 (d, ³J = 7 Hz, 6H, H-29, H-30). ¹³C {¹H} NMR (100.57 MHz, CDCl₃); δ (ppm) 188.0 (C-18), 165.8 (C-19/C-20), 165.1 (C-19/C-20), 142.2 (C-9), 135.6 (C-2), 134.7 (C-7/C-17), 134.3 (C-7/C-17), 129.1 (C-12/C-13/C-15/C-16), 128.6 (C-14), 128.4 (C-12/C-13/C-15/C-16), 125.9 (C-10), 124.0 (C-4, C-5), 112.5 (C-3/C-6), 110.1 (C-3/C-6), 109.7 (C-27), 98.2 (C-22), 85.4 (C-25/C-26), 85.1 (C-25/C-26), 82.5 (C-23/C-24), 82.4 (C-23/C-24), 54.4 (C-11), 44.9 (C-8), 34.4 (C-1), 31.6 (C-28), 22.7 (C-29, C-30), 18.8 (C-21).

General procedure for the syntheses of compounds **2 c–5 d**

Silver(I) oxide (1.38 mol equiv.) was added to a solution of compounds **c** or **d** (2.25 mol equiv.) dissolved in dichloromethane and stirred at 40 °C for 4 h in darkness. A solution of [M^{III}(cym/Cp*)Cl₂]₂ (1.00 mol equiv.) in dichloromethane was added and the

mixture was stirred at 40 °C for 24 h in darkness. A solution of ammonium hexafluorophosphate (6.75–7.86 mol equiv.) dissolved in methanol (ca. 15 mL) was added to the mixture and allowed to stir for a further 3 h in darkness. The solvents were evaporated and dichloromethane (ca. 25 mL) was added. The resultant suspension was filtered through a celite pad (ca. 10 cm) and fractions were collected after elution with either dichloromethane, acetonitrile, or methanol depending on the compound. The solvent was evaporated, the crude product was dissolved in a minimal amount of dichloromethane and the compound was precipitated by addition of *n*-hexane. The precipitate was dried *in vacuo* to obtain the pure complexes.

[Chlorido{1-[(1-benzyl-1,2,3-triazol-4-yl-κN)methyl]-3-2-methylimidazole-ylidene-κC}(η⁶-p-cymene)ruthenium(II)] hexafluorophosphate 2c

The synthesis of **2c** was performed according to the general procedure using silver(I) oxide (38 mg, 0.16 mmol), **c** (106 mg, 0.26 mmol), [Ru(cym)Cl₂]₂ (72 mg, 0.12 mmol), and ammonium hexafluorophosphate (151 mg, 0.93 mmol). The celite pad was washed with dichloromethane (ca. 100 mL) and acetonitrile (ca. 250 mL) was used as an eluent to collect the fraction to afford a yellow powder (27 mg, 17%). Single crystals suitable for X-ray diffraction analysis were grown from acetonitrile/toluene after performing a reaction between [Ru(cym)Cl₂]₂ and **c** to yield the complex with a chloride counterion (**2c^{Cl}**). Calcd. for C₂₄H₂₉ClF₆N₅PRu: C, 43.09; H, 4.37; N, 10.47%. Found: C, 43.47; H, 3.98; N, 10.11%. MS (ESI⁺): *m/z* 524.1155 [M–PF₆]⁺ (*m*_{calc} = 524.1151). ¹H NMR (399.89 MHz, CDCl₃); δ (ppm) 7.69 (s, 1H, H-6), 7.41–7.34 (m, 3H, H-9, H-10, H-11), 7.34–7.29 (m, 2H, H-8, H-12), 7.17 (d, ⁴*J* = 2 Hz, 1H, H-2), 7.05 (d, ⁴*J* = 2 Hz, 1H, H-3), 5.67 (d, ³*J* = 6 Hz, 1H, H-17/H-18), 5.60–5.55 (m, 4H, H-7a, H-7b, H-17/H-18, H-19/H-20), 5.33 (d, ³*J* = 6 Hz, 1H, H-19/H-20), 5.29 (d, ²*J*_{H–H^r} = 16 Hz, 1H, H-4a/b), 4.98 (d, ²*J*_{H–H^r} = 16 Hz, 1H, H-4a/b), 3.96 (s, 3H, H-1), 2.78 (sept, ³*J* = 7 Hz, 1H, H-22), 2.12 (s, 3H, H-15), 1.22 (d, ³*J* = 7 Hz, 3H, H-23/H-24), 1.20 (d, ³*J* = 7 Hz, 3H, H-23/H-24). ¹³C{¹H} NMR (100.57 MHz, CDCl₃); δ (ppm) 173.0 (C-14), 141.9 (C-5), 132.8 (C-13), 129.5 (C-9, C-10, C-11), 128.8 (C-8, C-12), 123.8 (C-2/C-3), 123.6 (C-6), 123.3 (C-2/C-3), 111.9 (C-21), 101.6 (C-16), 87.4 (C-17/C-18/C-19/C-20), 87.3 (C-17/C-18/C-19/C-20), 86.7 (C-17/C-18/C-19/C-20), 83.8 (C-17/C-18/C-19/C-20), 56.0 (C-7), 44.5 (C-4), 38.4 (C-1), 31.4 (C-22), 23.5 (C-23/C-24), 21.4 (C-23/C-24), 19.1 (C-15).

[Chlorido{1-[(1-benzyl-1,2,3-triazol-4-yl-κN)methyl]-3-methylimidazole-2-ylidene-κC}(η⁶-p-cymene)osmium(II)] hexafluorophosphate 3c

The synthesis of **3c** was performed according to the general procedure using silver(I) oxide (42 mg, 0.18 mmol), **c** (118 mg, 0.30 mmol), [Os(cym)Cl₂]₂ (104 mg, 0.13 mmol), and ammonium hexafluorophosphate (169 mg, 1.04 mmol). The celite pad was washed with dichloromethane (ca. 100 mL) followed by a mixture of dichloromethane and methanol (ca. 100 mL, 9:1). The latter fraction was collected and evaporated to afford a yellow powder (77 mg, 38%). Calcd. for C₂₄H₂₉ClF₆N₅OsP·0.2H₂O: C, 37.84; H, 3.89; N, 9.19%. Found: C, 38.00; H, 4.03; N, 9.01%. HRMS (ESI⁺): *m/z* 614.1722 [M–PF₆]⁺ (*m*_{calc} = 614.1726). ¹H NMR (399.89 MHz, CDCl₃); δ (ppm) 7.74 (s, 1H, H-6), 7.41–7.35 (m, 3H, H-9, H-10, H-11), 7.35–7.30 (m, 2H, H-8, H-12), 7.11 (d, ⁴*J* = 2 Hz, 1H, H-2/H-3), 6.98 (d, ⁴*J* = 2 Hz, 1H, H-2/H-3), 5.72 (d, ³*J* = 6 Hz, 1H, H-17/H-18), 5.66 (dd, ²*J* = 13 Hz, ³*J* = 5.5 Hz, 2H, H-17/H-18, H-19/H-20), 5.59 (d, ³*J* = 4 Hz, 2H, H-7a, H-7b), 5.51 (d, ³*J* = 6 Hz, 1H, H-19/H-20), 5.33 (d, ²*J*_{H–H^r} = 16 Hz, 1H, H-4a/b), 4.98 (d, ²*J*_{H–H^r} = 16 Hz, 1H, H-4a/b), 3.92 (s, 3H, H-1), 2.71 (sept, ³*J* = 7 Hz, 1H, H-22), 2.24 (s, 3H, H-15), 1.23 (d, ³*J* = 7 Hz,

3H, H-23/H-24), 1.17 (d, ³*J* = 7 Hz, 3H, H-23/H-24). ¹³C{¹H} NMR (100.57 MHz, CDCl₃); δ (ppm) 157.9 (C-14), 140.5 (C-5), 132.9 (C-13), 129.5 (C-9, C-10, C-11), 128.8 (C-8, C-12), 123.3 (C-6), 122.8 (C-2/C-3), 122.2 (C-2/C-3), 102.4 (C-21), 93.2 (C-15), 78.9 (C-17/C-18/C-19/C-20), 78.5 (C-17/C-18/C-19/C-20), 78.1 (C-17/C-18/C-19/C-20), 74.9 (C-17/C-18/C-19/C-20), 55.9 (C-7), 44.7 (C-4), 38.3 (C-1), 31.4 (C-22), 24.0 (C-23/C-24), 21.5 (C-23/C-24), 19.1 (C-15).

[Chlorido{1-[(1-benzyl-1,2,3-triazol-4-yl-κN)methyl]-3-methylimidazole-2-ylidene-κC}(η⁵-pentamethylcyclopentadienyl)rhodium(III)] hexafluorophosphate 4c

The synthesis of **4c** was performed according to the general procedure using silver(I) oxide (50 mg, 0.22 mmol), **c** (118 mg, 0.30 mmol), [Rh(Cp^{*})Cl₂]₂ (97 mg, 0.16 mmol), and ammonium hexafluorophosphate (173 mg, 1.06 mmol). The celite pad was washed with dichloromethane (ca. 100 mL), followed by a mixture of dichloromethane and methanol (ca. 100 mL, 9:1). The latter fraction was collected and evaporated to afford an orange powder (21 mg, 22%). Calcd. for C₂₄H₃₀ClF₆N₅Prh·0.45H₂O·0.25 C₆H₁₄: C, 43.66; H, 4.94; N, 9.98%. Found: C, 43.60; H, 4.89; N, 9.97%. MS (ESI⁺): *m/z* 526.1249 [M–PF₆]⁺ (*m*_{calc} = 526.1245). ¹H NMR (399.89 MHz, CDCl₃); δ (ppm) 7.89 (s, 1H, H-6), 7.38–7.34 (m, 3H, H-9, H-10, H-11), 7.34–7.30 (m, 2H, H-8, H-12), 7.26 (d, ⁴*J* = 2 Hz, 1H, H-2/H-3), 7.06 (d, ⁴*J* = 2 Hz, 1H, H-2/H-3), 5.63 (d, ²*J*_{H–H^r} = 14 Hz, 1H, H-7a/b), 5.58 (d, ²*J*_{H–H^r} = 14 Hz, 1H, H-7a/b), 5.44 (d, ²*J*_{H–H^r} = 17 Hz, 1H, H-4a/b), 4.96 (d, ²*J*_{H–H^r} = 17 Hz, 1H, H-4a/b), 3.92 (s, 3H, H-1), 1.66 (s, 15H, H-15). ¹³C{¹H} NMR (100.57 MHz, CDCl₃); δ (ppm) 168.1 (d, ¹*J*(Rh–C) = 50 Hz, C-14), 141.7 (C-5), 133.0 (C-13), 129.5 (C-9, C-10, C-11), 128.7 (C-8, C-12), 124.4 (C-6), 124.1 (C-2/C-3), 124.0 (C-2/C-3), 98.6 (d, ¹*J*(Rh–C_{cp}) = 7 Hz, C-16), 56.0 (C-7), 44.2 (C-4), 38.1 (C-1), 9.6 (C-15).

[Chlorido{1-[(1-benzyl-1,2,3-triazol-4-yl-κN)methyl]-3-methylimidazole-2-ylidene-κC}(η⁵-pentamethylcyclopentadienyl)iridium(III)] hexafluorophosphate 5c

The synthesis of **5c** was performed according to the general procedure using silver(I) oxide (43 mg, 0.19 mmol), **c** (121 mg, 0.30 mmol), [Ir(Cp^{*})Cl₂]₂ (108 mg, 0.13 mmol), and ammonium hexafluorophosphate (173 mg, 1.06 mmol). The celite pad was washed with dichloromethane (ca. 100 mL), followed by a mixture of dichloromethane and methanol (ca. 100 mL, 9:1). The latter fraction was collected and evaporated to afford a yellow powder (97 mg, 47%). Single crystals suitable for X-ray diffraction analysis were grown from water/methanol. Calcd. for C₂₄H₃₀ClF₆IrN₅P: C, 37.87; H, 3.97; N, 9.20%. Found: C, 38.13; H, 3.90; N, 8.92%. MS (ESI⁺): *m/z* 616.1811 [M–PF₆]⁺ (*m*_{calc} = 616.1819). ¹H NMR (399.89 MHz, CDCl₃); δ (ppm) 7.92 (s, 1H, H-6), 7.40–7.34 (m, 3H, H-9, H-10, H-11), 7.34–7.30 (m, 2H, H-8, H-12), 7.24 (d, ⁴*J* = 2 Hz, 1H, H-2/H-3), 7.04 (d, ⁴*J* = 2 Hz, 1H, H-2/H-3), 5.64 (d, ²*J*_{H–H^r} = 15 Hz, 1H, H-7a/b), 5.59 (d, ²*J*_{H–H^r} = 15 Hz, 1H, H-7a/b), 5.42 (d, ²*J*_{H–H^r} = 16 Hz, 1H, H-4a/b), 4.86 (d, ²*J*_{H–H^r} = 16 Hz, 1H, H-4a/b), 3.89 (s, 3H, H-1), 1.69 (s, 15H, H-15). ¹³C{¹H} NMR (100.57 MHz, CDCl₃); δ (ppm) 153.2 (C-14), 140.8 (C-5), 132.9 (C-13), 129.5 (C-9, C-10, C-11), 128.7 (C-8, C-12), 124.2 (C-6), 123.1 (C-2, C-3), 91.2 (C-16), 56.1 (C-7), 44.5 (C-4), 37.5 (C-1), 9.4 (C-15).

[Chlorido{1-[(1-benzyl-1,2,3-triazol-4-yl-κN)methyl]-3-methylbenzimidazole-2-ylidene-κC}(η⁶-p-cymene)ruthenium(II)] hexafluorophosphate 2d

The synthesis of **2d** was performed according to the general procedure using silver(I) oxide (47 mg, 0.20 mmol), **d** (150 mg, 0.33 mmol), [Ru(cym)Cl₂]₂ (91 mg, 0.15 mmol), and ammonium hexafluorophosphate (163 mg, 1.00 mmol). The celite pad was washed with dichloromethane (ca. 100 mL) and acetonitrile (ca. 250 mL) was

used as an eluent to collect the fraction to afford an orange powder (107 mg, 50%). Single crystals suitable for X-ray diffraction analysis were grown from acetonitrile/toluene after performing a reaction between $[\text{Ru}(\text{cym})\text{Cl}_2]_2$ and **d** to yield the complex with a chloride counterion (**2d^{Cl}**). Calcd. for $\text{C}_{28}\text{H}_{31}\text{ClF}_6\text{N}_5\text{PRu}$: C, 46.48; H, 4.39; N, 9.68%. Found: C, 46.36; H, 4.47; N, 9.82%. MS (ESI⁺): m/z 574.1301 $[\text{M}-\text{PF}_6]^{+}$ ($m_{\text{calc}} = 574.1311$). ¹H NMR (399.89 MHz, CDCl₃); δ (ppm) 7.79 (s, 1H, H-10), 7.57–7.54 (m, 1H, H-3), 7.46–7.42 (m, 1H, H-6), 7.40–7.34 (m, 5H, H-4, H-4, H-13, H-14, H-15), 7.34–7.30 (m, 2H, H-12, H-16), 5.79 (d, ³ $J = 6$ Hz, 1H, H-21/H-22), 5.72 (d, ² $J_{\text{H}-\text{H}'} = 16$ Hz, 1H, H-8a/b), 5.69–5.66 (m, 1H, H-21/H-22), 5.65–5.62 (m, 2H, H-11a/b, H-23/H-24), 5.56 (d, ² $J_{\text{H}-\text{H}'} = 15$ Hz, 1H, H-11a/b), 5.44 (d, ³ $J = 6$ Hz, 1H, H-23/H-24), 5.08 (d, ² $J_{\text{H}-\text{H}'} = 16$ Hz, 1H, H-8a/b), 4.17 (s, 3H, H-1), 2.52 (sept, ³ $J = 7$ Hz, 1H, H-26), 2.13 (s, 3H, H-19), 1.25 (d, ⁴ $J = 2$ Hz, 3H, H-27/H-28), 1.24 (d, ⁴ $J = 2$ Hz, 3H, H-27/H-28). ¹³C{¹H} NMR (100.57 MHz, CDCl₃); δ (ppm) 187.3 (C-18), 141.7 (C-9), 135.3 (C-2), 134.0 (C-7), 132.7 (C-17), 129.5 (C-13, C-14, C-15), 128.9 (C-12, C-16), 124.4 (C-4/C-5), 124.2 (C-4/C-5), 124.0 (C-10), 113.4 (C-25), 110.4 (C-6), 110.1 (C-3), 102.0 (C-20), 88.4 (C-21/C-22), 88.0 (C-21/C-22), 87.8 (C-23/C-24), 84.3 (C-23/C-24), 56.0 (C-11), 40.8 (C-8), 35.5 (C-1), 31.4 (C-26), 23.6 (C-28), 21.3 (C-27), 19.2 (C-19).

[Chlorido{1-[(1-benzyl-1,2,3-triazol-4-yl- κ N)methyl]-3-methylbenzimidazole-2-ylidene- κ C}(\eta^5\text{-p-cymene)osmium(III)}] \text{hexafluorophosphate } 3\text{d}

The synthesis of **3d** was performed according to the general procedure using silver(I) oxide (47 mg, 0.20 mmol), **d** (150 mg, 0.33 mmol), $[\text{Os}(\text{cym})\text{Cl}_2]_2$ (117 mg, 0.15 mmol), and ammonium hexafluorophosphate (163 mg, 1.00 mmol). The celite pad was washed with dichloromethane (ca. 100 mL) and acetonitrile (ca. 250 mL) was used as an eluent to collect the fraction to afford a light brown powder (124 mg, 52%). Calcd. for $\text{C}_{28}\text{H}_{31}\text{ClF}_6\text{N}_5\text{OsP}$: C, 41.61; H, 3.87; N, 8.67%. Found: C, 41.39; H, 3.59; N, 8.51%. MS (ESI⁺): m/z 664.1860 $[\text{M}-\text{PF}_6]^{+}$ ($m_{\text{calc}} = 664.1883$). ¹H NMR (399.89 MHz, CDCl₃); δ (ppm) 7.83 (s, 1H, H-10), 7.56 (d, ³ $J = 8$ Hz, 1H, H-3), 7.42–7.29 (m, 8H, H-4, H-5, H-6, H-12, H-13, H-14, H-15, H-16), 5.82 (d, ³ $J = 6$ Hz, 1H, H-23/H-24), 5.79–5.69 (m, 3H, H-8a/b, H-21/H-22, H-23/H-24), 5.63 (d, ² $J_{\text{H}-\text{H}'} = 23$ Hz, 2H, H-11a, H-11b), 5.58 (d, ³ $J = 9$ Hz, 1H, H-21/H-22), 5.07 (d, ² $J_{\text{H}-\text{H}'} = 16$ Hz, 1H, H-8a/b), 4.12 (s, 3H, H-1), 2.80 (sept, ³ $J = 7$ Hz, 1H, H-26), 2.26 (s, 3H, H-19), 1.27 (d, ³ $J = 7$ Hz, 3H, H-27/H-28), 1.19 (d, ³ $J = 7$ Hz, 3H, H-27/H-28). ¹³C{¹H} NMR (100.57 MHz, CDCl₃); δ (ppm) 171.1 (C-18), 140.3 (C-9), 134.9 (C-2), 133.4 (C-7), 132.7 (C-17), 129.5 (C-13, C-14, C-15), 128.9 (C-12, C-16), 124.5 (C-4, C-5), 124.1 (C-10), 110.7 (C-6), 110.3 (C-3), 104.2 (C-25), 93.6 (C-20), 79.9 (C-23/C-24), 79.5 (C-23/C-24), 79.2 (C-21/C-22), 75.5 (C-21/C-22), 56.0 (C-11), 41.2 (C-8), 35.4 (C-1), 31.3 (C-26), 23.9 (C-28), 21.3 (C-27), 19.2 (C-19).

[Chlorido{1-[(1-benzyl-1,2,3-triazol-4-yl- κ N)methyl]-3-methylbenzimidazole-2-ylidene- κ C}(\eta^5\text{-pentamethylcyclopentadienyl)rhodium(III)}] \text{hexafluorophosphate } 4\text{d}

The synthesis of **4d** was performed according to the general procedure using silver(I) oxide (33 mg, 0.14 mmol), **d** (105 mg, 0.23 mmol), $[\text{Rh}(\text{Cp}^*)\text{Cl}_2]_2$ (64 mg, 0.10 mmol), and ammonium hexafluorophosphate (133 mg, 0.82 mmol). The celite pad was washed with dichloromethane (ca. 100 mL), followed by a mixture of dichloromethane and methanol (ca. 100 mL, 9:1). The latter fraction was collected and evaporated to afford an orange powder (47 mg, 31%). Calcd. for $\text{C}_{28}\text{H}_{32}\text{ClF}_6\text{N}_5\text{PRh} \cdot 0.4\text{H}_2\text{O}$: C, 46.12; H, 4.53; N, 9.61%. Found: C, 46.29; H, 4.62; N, 9.42%. MS (ESI⁺): m/z 576.1406 $[\text{M}-\text{PF}_6]^{+}$ ($m_{\text{calc}} = 576.1396$). ¹H NMR (399.89 MHz, CDCl₃); δ (ppm) 8.03 (s, 1H, H-10), 7.70 (d, ³ $J = 8$ Hz, 1H, H-3), 7.48–7.32 (m, 8H, H-4, H-5, H-6, H-12, H-13, H-14, H-15, H-16), 5.92 (d, ² $J_{\text{H}-\text{H}'} = 16$ Hz, 1H, H-8a/b), 5.65 (d, ² $J_{\text{H}-\text{H}'} = 14$ Hz, 1H, H-11a/b), 5.59 (d,

² $J_{\text{H}-\text{H}'} = 14$ Hz, 1H, H-11a/b), 5.07 (d, ² $J_{\text{H}-\text{H}'} = 17$ Hz, 1H, H-8a/b), 4.13 (s, 3H, H-1), 1.71 (s, 15H, H-19). ¹³C{¹H} NMR (100.57 MHz, CDCl₃); δ (ppm) 181.2 (d, ¹ $J_{\text{Rh}-\text{C}(\text{NHC})} = 50$ Hz, C-18), 141.5 (C-9), 135.2 (C-2), 134.3 (C-7), 132.7 (C-17), 129.6 (C-13, C-14, C-15), 128.8 (C-12, C-16), 125.0 (C-10), 124.6 (C-4, C-5), 111.0 (C-3), 110.6 (C-6), 99.3 (d, ¹ $J(\text{Rh}-\text{C}_{\text{cp}}) = 7$ Hz, C-20), 56.2 (C-11), 40.7 (C-8), 35.2 (C-1), 9.7 (C-19).

[Chlorido{1-[(1-benzyl-1,2,3-triazol-4-yl- κ N)methyl]-3-methylbenzimidazole-2-ylidene- κ C}(\eta^5\text{-pentamethylcyclopentadienyl)iridium(III)}] \text{hexafluorophosphate } 5\text{d}

The synthesis of **5d** was performed according to the general procedure using silver(I) oxide (47 mg, 0.20 mmol), **d** (149 mg, 0.33 mmol), $[\text{Ir}(\text{Cp}^*)\text{Cl}_2]_2$ (117 mg, 0.15 mmol), and ammonium hexafluorophosphate (189 mg, 1.16 mmol). The celite pad was eluted with dichloromethane (ca. 200 mL) and the fraction was collected to afford a yellow powder (158 mg, 66%). Single crystals suitable for X-ray diffraction analysis were grown from chloroform. Calcd. for $\text{C}_{28}\text{H}_{32}\text{ClF}_6\text{IrN}_5\text{P} \cdot 0.25\text{C}_6\text{H}_{14}$: C, 42.55; H, 4.30; N, 8.41%. Found: C, 42.69; H, 4.20; N, 8.26%. HRMS (ESI⁺): m/z 666.1963 $[\text{M}-\text{PF}_6]^{+}$ ($m_{\text{calc}} = 666.1970$). ¹H NMR (399.89 MHz, CDCl₃); δ (ppm) 8.07 (s, 1H, H-10), 7.69 (d, ³ $J = 8$ Hz, 1H, H-3), 7.46–7.40 (m, 2H, H-4, H-6), 7.40–7.32 (m, 6H, H-5, H-12, H-13, H-14, H-15, H-16), 5.89 (d, ² $J_{\text{H}-\text{H}'} = 17$ Hz, 1H, H-8a/b), 5.66 (d, ² $J_{\text{H}-\text{H}'} = 15$ Hz, 1H, H-11a/b), 5.60 (d, ² $J_{\text{H}-\text{H}'} = 15$ Hz, 1H, H-11a/b), 4.96 (d, ² $J_{\text{H}-\text{H}'} = 17$ Hz, 1H, H-8a/b), 4.09 (s, 3H, H-1), 1.74 (s, 15H, H-19). ¹³C{¹H} NMR (100.57 MHz, CDCl₃); δ (ppm) 165.5 (C-18), 140.7 (C-9), 135.0 (C-2), 133.8 (C-7), 132.7 (C-17), 129.7 (C-13/C-14/C-15), 129.6 (C-13/C-14/C-15), 128.8 (C-12, C-16), 125.0 (C-4/C-5), 124.8 (C-10), 124.6 (C-4/C-5), 111.0 (C-3/C-6), 110.8 (C-3/C-6), 92.0 (C-20), 56.2 (C-11), 40.9 (C-8), 34.7 (C-1), 9.4 (C-19).

Stability studies

For stability studies in DMSO, **5c** (1–2 mg) was dissolved in DMSO-*d*₆ and ¹H NMR spectra were recorded for 120 h. To determine the stability in aqueous solution, **2c–5c** (1–2 mg) were dissolved in DMSO-*d*₆, diluted with D₂O to reach a DMSO-*d*₆ content of 15%, and ¹H NMR spectra were recorded for 120 h. For **5c**, 1 equiv. of AgNO₃ was added after 120 h to confirm the completion of the chlorido/aqua exchange. To determine the possible formation of a DMSO complex of **5c**, the compound (2 mg) was dissolved in DMSO-*d*₆ and its ¹H NMR spectrum was recorded. After 2 h, a small portion was taken from the sample and diluted with D₂O to reach a DMSO-*d*₆ content of 15%, and ¹H NMR spectra were recorded for 4 h. AgNO₃ (2 eq.) was added after 4 h. Furthermore, a ¹H NMR spectrum of **5c** (2 mg) dissolved in CDCl₃ was recorded. DMSO (2 eq.) was then added to the sample and ¹H NMR spectra were recorded after 0, 2, and 4 h. After 4 h, more DMSO (8 eq.) was added and the ¹H NMR spectrum was recorded.

To evaluate the ligand exchange reaction over longer periods, **2c–4c** were dissolved in DMSO-*d*₆, diluted with D₂O to reach a DMSO-*d*₆ content of 15%, and 1.5 equiv. of AgNO₃ were added immediately. An additional 1.5 equiv. of AgNO₃ were added after 24 h and the reaction was monitored by ¹H NMR spectroscopy for 30 d.

Biomolecule interaction studies

The biomolecule interactions of **2c–5c** were studied by ¹H NMR spectroscopy. All complexes were initially dissolved in MeOD-*d*₄ and diluted with D₂O to obtain solutions in 20% MeOD-*d*₄/D₂O. L-Methionine, L-cysteine, L-histidine, and 9-ethylguanine were dissolved in MeOD-*d*₄ and diluted with D₂O to obtain solutions in 20% MeOD-*d*₄/D₂O. Equimolar amounts of the biomolecule solutions were added to each complex and ¹H NMR spectra were recorded

for 48 h. After 48 h, an additional equivalent of the respective biomolecule solution was added to each complex and ^1H NMR spectra were recorded.

X-ray fluorescence microscopy (XFM)

Sample preparation. Silicon nitride membranes (Silson Ltd, Warwickshire, England) were washed for 2 min each in Milli-Q water, 70% ethanol, and 100% ethanol in a small Petri dish. The membranes were air-dried under sterile conditions and transferred into wells of 12-well culture plates, which were exposed to UV-light overnight. A549 cells were kindly provided by Dr. Judy Li and Dr. Alex Staudacher from the Hanson Institute at University of South Australia (passage 32). SKOV-3 cells were kindly provided by Dr. Carmela Ricciardelli from the Robinson Research Institute at The University of Adelaide, Australia. The cells were cultured in a T75 flask and were collected after trypsinizing (0.25% trypsin and ethylenediaminetetraacetic acid) for 3 min. The cells were spun down at 1,200 rpm for 5 min. Cell supernatant was discarded and the pellet was suspended in 1 mL culturing media (A549: RPMI 1640, 5% FCS, and 1% penicillin/streptomycin; SKOV-3: DMEM/F12, 10% FCS, L-glutamine, 1% penicillin/streptomycin and 0.1% fungizone). Cell suspensions were mixed with trypan blue solution (0.4%) and transferred into a cell counting chamber slide (Invitrogen). The cells were counted with Countess II (Life Technologies). The cell solutions were prepared with culturing media, and A549 (2,450) and SKOV-3 cells (2,000) were seeded onto each membrane without making contact with the pipette tip. The cells were incubated for 3 h at 37 °C and 5% CO_2 atmosphere for attachment. Culturing media (1.4 mL) was added carefully to each well, and the cells were incubated overnight at 37 °C, 5% CO_2 .

Metal complex incubation. **5d** (30 μM , 1% DMSO in media) was added to the wells carefully in 2 separate portions of 0.7 mL, enough to soak the cell-coated silicon nitride membrane in solution. The cells were incubated for 4 h. The compound solution was aspirated from the well carefully, avoiding contact with the membrane, then the membrane was washed with PBS (0.7 mL) and aspirated. The cells were fixed onto the membrane with 4% buffered paraformaldehyde (0.7 mL). After 5 min, the paraformaldehyde solution was aspirated. The membrane was washed with PBS (0.7 mL) and aspirated. A solution of ammonium acetate (100 mM, 0.7 mL) was added to the membrane carefully and soaked for 2 min, after which ammonium acetate was aspirated. The latter step was repeated before Milli-Q water (0.7 mL) was added to cover the surface of the membrane and to wash out excess ammonium acetate. The membrane was then allowed to dry slowly while covered. The membrane was stored at room temperature for subsequent experimentation.

Australian Synchrotron instrumentation and operating conditions. The distributions of Zn and Ir in A549 cells incubated with **5d** were mapped at the XFM beamline at the Australian Synchrotron (Clayton VIC, Australia) with modifications to the protocol described previously.^[29] The beam was tuned to an incident energy of 15.8 keV using a Si(111) monochromator and focused to $\sim 1.5 \mu\text{m}$ using a Kirkpatrick-Baez mirror pair. A 384-element silicon array detector (Maia 384; Brookhaven National Laboratory, Upton, NY and CSIRO, Clayton, Victoria, Australia) in 180° backscatter geometry was used to collect the fluorescence signal from the samples with a dwell time of 80–200 ms/point. Analysis of XRF data was performed using the Dynamic Analysis method as implemented in the GeoPIXE software package.

Advanced Photon Source instrumentation and operating conditions. The distributions of Zn, and Ir in SKOV-3 cells incubated with **5d** were mapped at the 2-ID-D beamline at the Advanced Photon

Source (Argonne National Laboratory, Lemont, IL) with modifications to the protocol described previously.^[30] A double multilayer monochromator and a gold “high flux” zone plate setup was used to focus a monochromatic beam into a spot of 300–400 nm FWHM in diameter. Cells treated with **5d** were imaged with an incident X-ray energy of 13.1 keV to excite at the L-edge of Ir; the P and Zn maps for these cells were generated from K-edge fluorescence of these elements. An energy-dispersive silicon drift detector (Vortex EM, SII Nanotechnology, Northridge, California, USA) was used to collect the X-ray fluorescence spectra from the sample, which was placed in a He environment at an angle of 75° to the incident beam. All elemental maps were recorded in fly-scan mode, with a 0.5 μm step-size in x and y direction, and a 150 ms dwell time for the **5d**-treated cell maps. Elemental maps were generated with the MAPS software package^[31] by Gaussian fitting of the raw emission spectra for each image pixel. The Gaussian peaks were matched to characteristic X-ray emission lines to determine the fluorescence signal for each element. Quantification of the data (in $\mu\text{g}/\text{cm}^2$) was performed by comparing the X-ray fluorescence intensities to those from National Bureau of Standards thin film standards NBS-1832, NBS-1833 (National Bureau of Standards, Gaithersburg, MD, USA).

DFT calculations

GAUSSIAN 09 W^[18] was used to calculate the optimized ground state structures and frequencies for the different molecules by density functional theory (DFT) with the B3LYP–D3 hybrid exchange functional and a split basis set for C, H, N, Cl (6-31G(d,p)) and the transitional metal iridium, osmium, rhodium, and ruthenium (SDDAll) in vacuum. The SCRF (self-consistent reaction field) keyword was implemented for the optimization of the molecules in aqueous environment. This method is the integral equation formalism variant of the Polarizable Continuum Model (IEFPCM).^[32] The EmpiricalDispersion=GD3 keyword was implemented for the empirical dispersion correction for the optimization of the molecules.^[33] The frontier orbitals were viewed and obtained through the Avogadro software (version 1.2.0).^[34]

Acknowledgements

We thank the University of Auckland (University of Auckland Doctoral Scholarship to K.K.H.T. and the Faculty of Science Research and Development Fund) and the Cancer Research Trust New Zealand for financial support. K.K.H.T. is grateful for a Maurice Wilkins Centre COVID-19 PhD Student Stipend Extension. M. H. is supported by a Sir Charles Hercus Health Research Fellowship through the Health Research Council of New Zealand. We are grateful to Tanya Groutso for collecting the single crystal X-ray diffraction data, and Tony Chen and Mansa Nair for collecting the ESI-MS data. This research was undertaken in part using the XFM beamlines at the Australian Synchrotron, part of ANSTO. This research used resources of the Advanced Photon Source, a U.S. Department of Energy (DOE) Office of Science User Facility operated for the DOE Office of Science by Argonne National Laboratory under Contract No. DE-AC02-06CH11357. Travel funding to perform experiments at the Advanced Photon Source was provided by the International Synchrotron Access Program (ISAP) managed by the Australian Synchrotron, part of ANSTO, funded by the Australian Government.

Conflict of Interest

The authors declare no conflict of interest.

Keywords: anticancer activity · biomolecule reactions · bioorganometallics · coordination mode · intracellular distribution

- [1] M. N. Hopkinson, C. Richter, M. Schedler, F. Glorius, *Nature* **2014**, *510*, 485–496.
- [2] a) M. Scholl, S. Ding, C. W. Lee, R. H. Grubbs, *Org. Lett.* **1999**, *1*, 953–956; b) A. Nasr, A. Winkler, M. Tamm, *Coord. Chem. Rev.* **2016**, *316*, 68–124; c) C. Johnson, M. Albrecht, *Coord. Chem. Rev.* **2017**, *352*, 1–14; d) Janssen-Muller, C. Schlepphorst, F. Glorius, *Chem. Soc. Rev.* **2017**, *46*, 4845–4854; e) V. Charra, P. de Fremont, P. Braunstein, *Coord. Chem. Rev.* **2017**, *341*, 53–176; f) E. Peris, *Chem. Rev.* **2018**, *118*, 9988–10031.
- [3] a) K. J. Kilpin, S. Crot, T. Riedel, J. A. Kitchen, P. J. Dyson, *Dalton Trans.* **2014**, *43*, 1443–1448; b) J. J. Zhang, J. K. Muenzner, M. A. Abu el Maaty, B. Karge, R. Schobert, S. Wolff, I. Ott, *Dalton Trans.* **2016**, *45*, 13161–13168; c) W. K. Liu, R. Gust, *Coord. Chem. Rev.* **2016**, *329*, 191–213; d) N. Y. S. Lam, D. Truong, H. Burmeister, M. V. Babak, H. U. Holtkamp, S. Movassaghi, D. M. Ayine-Tora, A. Zafar, M. Kubanik, L. Oehninger, T. Söhnel, J. Reynisson, S. M. F. Jamieson, C. Gaiddon, I. Ott, C. G. Hartinger, *Inorg. Chem.* **2018**, *57*, 14427–14434.
- [4] a) A. Melaiye, R. S. Simons, A. Milsted, F. Pingitore, C. Wesdemiotis, C. A. Tessier, W. J. Youngs, *J. Med. Chem.* **2004**, *47*, 973–977; b) S. Medici, M. Peana, G. Crisponi, V. M. Nurchi, J. I. Lachowicz, M. Remelli, M. A. Zoroddu, *Coord. Chem. Rev.* **2016**, *327*, 349–359.
- [5] I. Fichtner, J. Cinatl, M. Michaelis, L. C. Sanders, R. Hilger, B. N. Kennedy, A. L. Reynolds, F. Hackenberg, G. Lally, S. J. Quinn, I. McRae, M. Tacke, *Lett. Drug Des. Discovery* **2012**, *9*, 815–822.
- [6] M. V. Baker, P. J. Barnard, S. J. Berners-Price, S. K. Brayshaw, J. L. Hickey, B. W. Skelton, A. H. White, *Dalton Trans.* **2006**, 3708–3715.
- [7] a) L. Mercs, M. Albrecht, *Chem. Soc. Rev.* **2010**, *39*, 1903–1912; b) L. Oehninger, M. Stefanopoulou, H. Alborzinia, J. Schur, S. Ludewig, K. Namikawa, A. Munoz-Castro, R. W. Koster, K. Baumann, S. Wolff, W. S. Sheldrick, I. Ott, *Dalton Trans.* **2013**, *42*, 1657–1666; c) L. Oehninger, R. Rubbiani, I. Ott, *Dalton Trans.* **2013**, *42*, 3269–3284; d) P. V. Simpson, C. Schmidt, I. Ott, H. Bruhn, U. Schatzschneider, *Eur. J. Inorg. Chem.* **2013**, *2013*, 5547–5554; e) F. Hackenberg, H. Müller-Bunz, R. Smith, W. Streciwilk, X. Zhu, M. Tacke, *Organometallics* **2013**, *32*, 5551–5560; f) V. Novohradsky, L. Zerzankova, J. Stepankova, A. Kisova, H. Kostrhunova, Z. Liu, P. J. Sadler, J. Kasparkova, V. Brabec, *Metallics* **2014**, *6*, 1491–1501.
- [8] M. P. Sullivan, M. K. Nieuwoudt, G. A. Bowmaker, N. Y. S. Lam, D. Truong, D. C. Goldstone, C. G. Hartinger, *Chem. Commun.* **2018**, *54*, 6120–6123.
- [9] B. T. Elie, Y. Pechenyy, F. Uddin, M. Contel, *J. Biol. Inorg. Chem.* **2018**, *23*, 399–411.
- [10] a) O. z. Karaca, V. Scalcon, S. M. Meier-Menches, R. Bonsignore, J. M. Brouwer, F. Tonolo, A. Folda, M. P. Rigobello, F. E. Kühn, A. Casini, *Inorg. Chem.* **2017**, *56*, 14237–14250; b) C. Schmidt, L. Albrecht, S. Balasubramanian, R. Misdeld, B. Karge, M. Brönstrup, A. Prokop, K. Baumann, S. Reichl, I. Ott, *Metallics* **2019**, *11*, 533–545; c) F. Guarra, N. Busto, A. Guerri, L. Marchetti, T. Marzo, B. García, T. Biver, C. Gabbiani, *J. Inorg. Biochem.* **2020**, 110998; d) R. Rubbiani, I. Kitanovic, H. Alborzinia, S. Can, A. Kitanovic, L. A. Onambele, M. Stefanopoulou, Y. Geldmacher, W. S. Sheldrick, G. Wolber, *J. Med. Chem.* **2010**, *53*, 8608–8618.
- [11] a) C. Wang, J. Liu, Z. Tian, M. Tian, L. Tian, W. Zhao, Z. Liu, *Dalton Trans.* **2017**, *46*, 6870–6883; b) Y. Han, X. Liu, Z. Tian, X. Ge, J. Li, M. Gao, Y. Li, Y. Liu, Z. Liu, *Chem. Asian J.* **2018**, *13*, 3697–3705; c) Y. Han, Z. Tian, S. Zhang, X. Liu, J. Li, Y. Li, Y. Liu, M. Gao, Z. Liu, *J. Inorg. Biochem.* **2018**, *189*, 163–171; d) Z. Xu, Y. Zhang, S. Zhang, X. Jia, G. Zhong, Y. Yang, Q. Du, J. Li, Z. Liu, *Cancer Lett.* **2019**, *447*, 75–85.
- [12] C. Chen, S. Ni, Q. Zheng, M. Yu, H. Wang, *Eur. J. Inorg. Chem.* **2017**, *2017*, 616–622.
- [13] a) K. Q. Vuong, M. G. Timerbulatova, M. B. Peterson, M. Bhadbhade, B. A. Messerle, *Dalton Trans.* **2013**, *42*, 14298–14308; b) P. M. Illam, S. Donthireddy, S. Chakraborty, A. Rit, *Organometallics* **2019**, *38*, 2610–2623; c) D. F. Wang, R. T. McBurney, I. Pernik, B. A. Messerle, *Dalton Trans.* **2019**, *48*, 13989–13999; d) S. Donthireddy, P. Mathoor Illam, A. Rit, *Inorg. Chem.* **2020**.
- [14] S. Movassaghi, S. Singh, A. Mansur, K. K. H. Tong, M. Hanif, H. U. Holtkamp, T. Söhnel, S. M. F. Jamieson, C. G. Hartinger, *Organometallics* **2018**, *37*, 1575–1584.
- [15] a) Y. He, M.-f. Lv, C. Cai, *Dalton Trans.* **2012**, *41*, 12428–12433; b) P. Zare, A. Stojanovic, F. Herbst, J. Akbarzadeh, H. Peterlik, W. H. Binder, *Macromolecules* **2012**, *45*, 2074–2084.
- [16] F. Saleem, G. K. Rao, S. Kumar, M. P. Singh, A. K. Singh, *Dalton Trans.* **2015**, *44*, 19141–19152.
- [17] K. K. H. Tong, M. Hanif, J. H. Lovett, K. Hummitzsch, H. H. Harris, T. Söhnel, S. M. F. Jamieson, C. G. Hartinger, *Molecules* **2020**, 25.
- [18] M. J. Frisch, G. W. Trucks, H. B. Schlegel, G. E. Scuseria, M. A. Robb, J. R. Cheeseman, G. Scalmani, V. Barone, G. A. Petersson, H. Nakatsuji, X. Li, M. Caricato, A. V. Marenich, J. Bloino, B. G. Janesko, R. Gomperts, B. Mennucci, H. P. Hratchian, J. V. Ortiz, A. F. Izmaylov, J. L. Sonnenberg, Williams, F. Ding, F. Lipparini, F. Egidi, J. Goings, B. Peng, A. Petrone, T. Henderson, D. Ranasinghe, V. G. Zakrzewski, J. Gao, N. Rega, G. Zheng, W. Liang, M. Hada, M. Ehara, K. Toyota, R. Fukuda, J. Hasegawa, M. Ishida, T. Nakajima, Y. Honda, O. Kitao, H. Nakai, T. Vreven, K. Throssell, J. A. Montgomery Jr., J. E. Peralta, F. Ogliaro, M. J. Bearpark, J. J. Heyd, E. N. Brothers, K. N. Kudin, V. N. Staroverov, T. A. Keith, R. Kobayashi, J. Normand, K. Raghavachari, A. P. Rendell, J. C. Burant, S. S. Iyengar, J. Tomasi, M. Cossi, J. M. Millam, M. Klene, C. Adamo, R. Cammi, J. W. Ochterski, R. L. Martin, K. Morokuma, O. Farkas, J. B. Foresman, D. J. Fox, Wallingford, CT, **2016**.
- [19] J. H. Lovett, H. H. Harris, *Curr. Opin. Chem. Biol.* **2021**, *61*, 135–142.
- [20] a) M. Hanif, A. A. Nazarov, C. G. Hartinger, W. Kandioller, M. A. Jakupec, V. B. Arion, P. J. Dyson, B. K. Keppler, *Dalton Trans.* **2010**, *39*, 7345–7352; b) M. Hanif, S. M. Meier, W. Kandioller, A. Bytzeck, M. Hejl, C. G. Hartinger, A. A. Nazarov, V. B. Arion, M. A. Jakupec, P. J. Dyson, B. K. Keppler, *J. Inorg. Biochem.* **2011**, *105*, 224–231.
- [21] a) Y. Fu, A. Habtemariam, A. M. B. H. Basri, D. Braddick, G. J. Clarkson, P. J. Sadler, *Dalton Trans.* **2011**, *40*, 10553–10562; b) I. Romero-Canelon, L. Salassa, P. J. Sadler, *J. Med. Chem.* **2013**, *56*, 1291–1300.
- [22] M. A. Bennett, A. K. Smith, *J. Chem. Soc. Dalton Trans.* **1974**, 233–241.
- [23] R. G. Ball, W. A. G. Graham, D. M. Heinekey, J. K. Hoyano, A. D. McMaster, B. M. Mattson, S. T. Michel, *Inorg. Chem.* **1990**, *29*, 2023–2025.
- [24] B. Booth, R. Haszeldine, M. Hill, *J. Chem. Soc. A* **1969**, 1299–1303.
- [25] M. A. Khalily, G. Gulseren, A. B. Tekinay, M. O. Guler, *Bioconjugate Chem.* **2015**, *26*, 2371–2375.
- [26] G. Sheldrick, *Acta Crystallogr. Sect. A* **2015**, *71*, 3–8.
- [27] a) O. V. Dolomanov, L. J. Bourhis, R. J. Gildea, J. A. Howard, H. Puschmann, *J. Appl. Crystallogr.* **2009**, *42*, 339–341; b) L. J. Bourhis, O. V. Dolomanov, R. J. Gildea, J. A. Howard, H. Puschmann, *Acta Crystallogr. Sect. A* **2015**, *71*, 59–75.
- [28] C. F. Macrae, I. Sovago, S. J. Cottrell, P. T. A. Galek, P. McCabe, E. Pidcock, M. Platings, G. P. Shields, J. S. Stevens, M. Towler, P. A. Wood, *J. Appl. Crystallogr.* **2020**, *53*, 226–235.
- [29] D. Truong, M. P. Sullivan, K. K. H. Tong, T. R. Steel, A. Prause, J. H. Lovett, J. W. Andersen, S. M. F. Jamieson, H. H. Harris, I. Ott, C. M. Weekley, K. Hummitzsch, T. Söhnel, M. Hanif, N. Metzler-Nolte, D. C. Goldstone, C. G. Hartinger, *Inorg. Chem.* **2020**, *59*, 3281–3289.
- [30] a) D. E. Morrison, J. B. Aitken, M. D. de Jonge, J. A. Ioppolo, H. H. Harris, L. M. Rendina, *Chem. Commun.* **2014**, *50*, 2252–2254; b) M. Busse, M. S. A. Windsor, A. J. Tefay, M. Kardashinsky, J. M. Fenton, D. E. Morrison, H. H. Harris, L. M. Rendina, *J. Inorg. Biochem.* **2017**, *177*, 313–321; c) C. M. Weekley, I. Kenkel, R. Lippert, S. Wei, D. Lieb, T. Cranwell, J. L. Wedding, A. S. Zillmann, R. Rohr, M. R. Filipovic, I. Ivanovic-Burmazovic, H. H. Harris, *Inorg. Chem.* **2017**, *56*, 6076–6093.
- [31] E. A. Carter, B. S. Rayner, A. I. McLeod, L. E. Wu, C. P. Marshall, A. Levina, J. B. Aitken, P. K. Witting, B. Lai, Z. Cai, S. Vogt, Y. C. Lee, C. I. Chen, M. J. Tobin, H. H. Harris, P. A. Lay, *Mol. Biosyst.* **2010**, *6*, 1316–1322.
- [32] G. Scalmani, M. J. Frisch, *J. Chem. Phys.* **2010**, *132*, 114110.
- [33] S. Grimme, J. Antony, S. Ehrlich, H. Krieg, *J. Chem. Phys.* **2010**, *132*, 154104.
- [34] M. D. Hanwell, D. E. Curtis, D. C. Lonie, T. Vandermeersch, E. Zurek, G. R. Hutchison, *J. Cheminf.* **2012**, *4*, 17.

Manuscript received: May 5, 2021

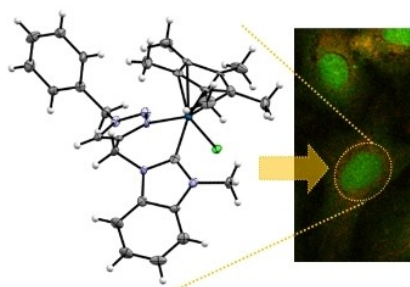
Revised manuscript received: June 16, 2021

Accepted manuscript online: July 1, 2021

Version of record online: ■■■, ■■■■

FULL PAPERS

Coordinated efforts against cancer: Organometallic Ru, Os, Rh, and Ir complexes of mono- or bidentately coordinating *N*-heterocyclic carbenes showed metal center-dependent cytotoxicity, with the Ir^{III} derivatives being the most potent anticancer agents *in vitro*. The biological activity seems related to the stability of the compounds in aqueous solution, together with the distinct reactivity to biomolecules.



K. K. H. Tong, Dr. M. Hanif, Dr. S. Movassaghi, Dr. M. P. Sullivan, J. H. Lovett, Dr. K. Hummitzsch, Prof. T. Söhnel, Dr. S. M. F. Jamieson, Prof. S. K. Bhargava, Prof. H. H. Harris, Prof. C. G. Hartinger*

1 – 11

Triazolyl-Functionalized *N*-Heterocyclic Carbene Half-Sandwich Compounds: Coordination Mode, Reactivity and *in vitro* Anticancer Activity

